

# Application of wavelet transform for the impulse response of pile

Sheng-Huoo Ni\*, Yu-Zhang Yang<sup>a</sup> and Chia-Rong Lyu

Department of Civil Engineering, National Cheng Kung University, Tainan, Taiwan 70101, ROC

(Received June 10, 2014, Revised March 20, 2017, Accepted March 22, 2017)

**Abstract.** The purpose of this paper is to study the capabilities of the impulse response method in length and flaw detecting for concrete piles and provide a suggested method to find small-size flaws in piles. In this work, wavelet transform is used to decompose the recorded time domain signal into a series of levels. These levels are narrowband, so the mix of different dominant bandwidths can be avoided. In this study, the impulse response method is used to analyze the signal obtained from the wavelet transform to improve the judgment of the flaw signal so as to detect the flaw location. This study provides a new way of thinking in non-destructive testing detection. The results show that the length of a pile is easy to be detected in the traditional reflection time or frequency domain method. However, the small flaws within pile are difficult to be found using these methods. The proposed approach in this paper is able to greatly improve the results of small-size flaw detection within piles by reducing the effects of any noise and clarifying the signal in the frequency domains.

**Keywords:** piles; impulse response method; signal processing; wavelet transform; non-destructive testing

## 1. Introduction

The NDT methods for pile integrity testing can be classified into two main types, namely the surface reflection method and the borehole method. Notably, sonic echo (SE) and impulse response (IR) methods, which are classified as surface reflection methods, have been used extensively to check the lengths and integrity of piles. It is more cost-effective than borehole methods. Among the related studies, only a few focus on the identifiable flaw in a pile and are summarized in Table 1. Of these studies, Kim *et al.* (2002, 2004) and Hartung *et al.* (1992) provide the most systematic investigations of the surface reflection method. Based on the impulse response test, Kim *et al.* (2002) demonstrated that the flaw size should be at least greater than 50% of the total cross-sectional area to be detectable, while Finno and Gassman (1998) indicated that a 25% flaw size can also be detected successfully. In the research of Hartung *et al.* (1992), when the sonic echo method was used for pile integrity detection, flaw sizes of more than 10% were indicated to be detectable. However, Lin *et al.* (1991) and Baker *et al.* (1991) show that a 15% flaw size is undetectable, while Kim *et al.* (2002) show that a flaw can be detected by the SE method when its size is larger than 30%. Clearly, an explicit limitation for both SE and IR methods in flaw size detection has not been unified in previous researches.

From the literature cited above, it can be seen that the surface reflected wave method can successfully be used to

detect the flaw size in a pile, but the conclusions are not consistent. Such result indicate that the professional judgment of testing personnel, differences between the various experimental conditions, the position of pile defects, and the relative stiffness of the surrounding soil are the most important influencing factors. The amount of reflected wave energy will directly affect the result of surface reflection pile integrity assessment (Berger and Cotton 1990, Stain 1982). Therefore, these factors should not be considered separately. Huang *et al.* (2010) and Ni *et al.* (2011) used a finite element simulation approach to discuss these factors and derived a formula which is capable of determining the minimum detectable flaw size with both the sonic echo and impulse response methods. However, in practical in-situ tests, the results were not as good as expected (Huang 2011).

Park *et al.* (2001) proposed a method of using harmonic wavelet transform to evaluate the dispersive phase and group velocities. This method introduces the idea of that the detailed information of signal can be found using the wavelet method. Similar idea was used to identify the damage of plates (Beheshti-Aval *et al.* 2011). Ni *et al.* (2012) proposed a new NDT method by utilizing the continuous wavelet transform (CWT) technique to enhance the determination of flaw signals. However, for signals that have limited data points, the continuous wavelet transform would produce redundant signals. The continue wavelet transform also has limitations of impracticality and redundancy. Because the limitations of CWT often cause error judgments, this study uses the discrete combined with the impulse response method to evaluate the defects in pile.

The purpose of this paper is to investigate three different types of small-size defect (10% of cross-sectional area) cases on in-situ test sites. The results of this paper will be compared to the results of the sonic echo method. Factors that could affect the applicability of the surface reflection

\*Corresponding author, Professor  
E-mail: [tonyni@mail.ncku.edu.tw](mailto:tonyni@mail.ncku.edu.tw)

<sup>a</sup> Graduate student  
E-mail: [n68981107@mail.ncku.edu.tw](mailto:n68981107@mail.ncku.edu.tw)

Table 1 Summary of published studies on the flaw detection in pile shafts using surface reflection methods

Reference	Flaw type	Model type	Flaw size (%)	Flaw depth ratio (diameter)	Analysis results
Baker <i>et al.</i> (1991)	Elliptical inclusion	Full size	15	2.9 (D = 0.9 m)	SE(N <sup>*1</sup> ), IR(N)
	Elliptical inclusion	Full size	15	3.77 (D = 0.9 m)	SE(YN <sup>*2</sup> ), IR(N)
	Necking	Full size	45	2.67 (D = 0.9 m)	SE(YN), IR(YN)
	Necking	Full size	45	13.11 (D = 0.9 m)	SE(YN), IR(Y <sup>*3</sup> )
	Nonaxisymmetric void	Full size	50	13.11 (D = 0.9 m)	SE(YN), IR(Y)
Briaud <i>et al.</i> (2002)	Necking	Full size	45	5.46 (D = 0.92 m)	SE(Y), IR(Y)
	Necking	Full size	63	9.51 (D = 0.92 m)	SE(N), IR(YN)
	Necking	Full size	43	19.67 (D = 0.92 m)	SE(YN), IR(YN)
	Necking	Full size	50	3.28 (D = 0.92 m)	SE(YN), IR(YN)
Finno and Gassman (1998b)	Necking	Full size	25	4.13 (D = 0.91 m)	IR(Y)
Hartung <i>et al.</i> (1992)	Axisymmetric void	Model shafts	10-50	13.04 (D = 0.05 m)	SE(Y)
Iskanker <i>et al.</i> (2003)	Necking	Full size	19	6 (D = 1.0 m)	SE(Y), IR(Y)
	Axisymmetric void	Model shafts	30-80	4 (D = 0.1 m)	SE(Y)
Kim <i>et al.</i> (2002)	Axisymmetric void	Model shafts	50-80	4 (D = 0.1 m)	IR(Y)
	Nonaxisymmetric void	Model shafts	30	6 (D = 0.1 m)	SE(Y), IR(YN)
Lin <i>et al.</i> (1991)	Axisymmetric void	FEM	75	5 (D = 0.4 m)	SE(Y), IR(Y)
	Central void	Full size	15	5.05 (D = 0.91 m)	IR(N)
	Necking	Full size	56	14.4 (D = 0.91 m)	IR(Y)
Sarhan <i>et al.</i> (2002)	Nonaxisymmetric void	Full size	10.67	2.8 (D = 0.762 m)	SE(N)
	Nonaxisymmetric void	Full size	14.4	3.0 (D = 0.762 m)	SE(Y)
	Nonaxisymmetric void	Full size	16.6	3.0 (D = 0.762 m)	SE(N)

\*<sup>1</sup>: no flaw was detected; \*<sup>2</sup>: a flaw was possibly detected; \*<sup>3</sup>: a flaw was detected

methods, including stiffness of the soil, type of mother wavelet, and the level of wavelet transform would not be covered and discussed in this paper.

## 2. Methodologies

### 2.1 Surface reflection method

The surface reflection method uses the wave reflected back from the location of the impedance change to evaluate the integrity of the piles. The sonic echo and impulse response methods are the two most popular ways for pile

nondestructive tests due to the advantages of speed, economy, and wide ranges. The surface reflection method is carried out by introducing a transient wave into a pile by striking the pile head with an impulse hammer and recording the vibration response of the pile with a geophone, which is also located on the top surface of the pile. The experimental schematic of the surface reflection method is shown in Fig. 1. The SE method interprets the transient response of the pile in the time domain while the impulse response analyzes it in the frequency domain.

In the sonic echo method, one geophone is placed on the top surface of the pile head to record the transient response of the pile. The recorded signal is then processed to find the

traveling time, phase direction, and amplitude. The velocity waveform in time domain is used to determine the depth of the impedance change in a pile, and this depth can be evaluated by the propagation velocity of the stress wave ( $V$ ) through the pile, and the travel time from the pile top to the interface of impedance change and back to the top. For the impulse response test, the impact force applied at the pile head should also be recorded. The IR method converts the impact force and transient response into the frequency domain using the Fast Fourier Transform (FFT) and then calculates the mobility, which is defined as the ratio of the velocity spectrum and the force spectrum. As shown in Fig. 2, to identify any repeated peaks in the mobility curve is the key to successfully using the impulse response method to evaluate the pile integrity. The resolution of impulse response signals can be defined in terms of the ratio  $P/Q$ . The higher the  $P/Q$  ratio is, the higher the signal resolution is, and the easier it is to distinguish the resonant peaks. This makes it easier to determine the pile length and the location of flaws (Finno and Gassman 1998a). The distance from the geophone to the source of the reflection ( $L$ ) can be correlated with the frequency difference ( $\Delta f$ ) between resonance peaks and wave velocity ( $V$ ) as shown below:

$$L = \frac{V}{2\Delta f} \tag{1}$$

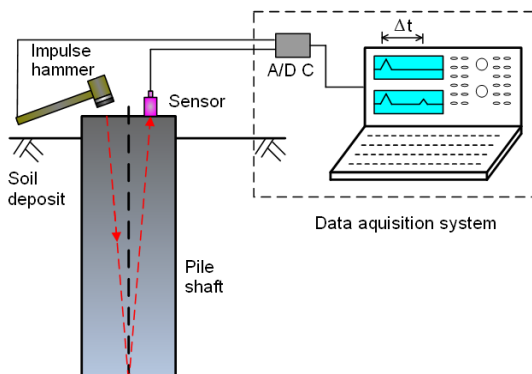


Fig. 1 Schematic depiction of the surface reflection method

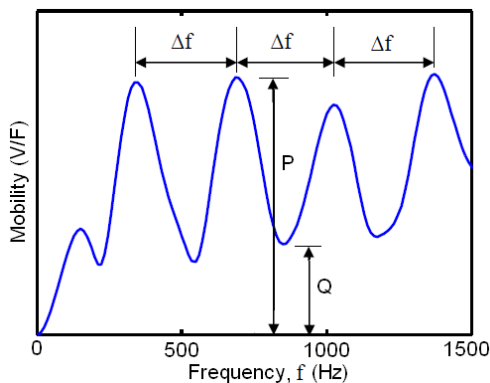


Fig. 2 Typical mobility plot obtained from an impulse response test

Table 2 Suggested compression wave velocity rating for concrete from ultrasonic test (From Malhotra 1976, Harrell and Stokoe 1984)

Compression wave velocity, m/sec (by Malhotra)	Compression wave velocity in a rod, m/sec (by Harrell and Stokoe)	General conditions
>4570	>4120	Excellent
3660 ~ 4570	3300 ~ 4120	Good
3050 ~ 3660	2750 ~ 3300	Questionable
2130 ~ 3050	1920 ~ 2750	Poor
< 2130	< 1920	Very poor

When the above equation condition is satisfied, the SE and IR methods will produce the same result. With the known pile length the wave propagation velocity can be back-calculated to be approximately 4000 m/sec. Also as illustrated in Table 2, the general conditions of excellence were chosen because they are pre-cast piles, and the corresponding wave propagation velocity is approximately 4000 m/sec. The wave propagation velocity of the tested pile was measured before the pile was installed into ground. The wave velocity of 4000 m/sec was used in this study.

### 2.2 Discrete wavelet transform

One of the major advantages of using wavelet transform is that the local features in the signals can be easily extracted. A wavelet is a waveform of limited duration that has an average value of zero. While Fourier transform breaks up signals into a series of sine-waves of various frequencies, wavelet transform breaks up a signal into shifted and scaled versions of the original wavelets. Two signals with the same spectral density could exhibit completely different transient characteristics (Newland, 1999). However, conventional Fourier analysis can only provide the spectral components of a signal and is independent of time. The scale ( $a$ ) and shift ( $\tau$ ) parameters are the core of the wavelet transform and lead to the construction of the time-frequency information.

There are two types of wavelet transform: continuous wavelets transform (CWT) and discrete wavelets transform (DWT), and both are continuous in time. CWT operates over every possible scale and translation whereas DWT use a specific subset of scale and translation values or representation grid (Addison, 2002). Wavelet coefficients,  $W_f$ , can be obtained by convoluting some proper wavelet function transform,  $\psi(t)$ , with input signal  $x(t)$  and is defined as follow

$$W_f(a, \tau) = \frac{1}{\sqrt{a}} \int x(t) \psi^* \left( \frac{t - \tau}{a} \right) dt \tag{2}$$

Where  $\psi^*(t)$  is the complex conjugate of  $\psi(t)$ . The above equation is known as continuous or discrete wavelet transforms if  $\tau$  and  $a$  are continuous, and discrete wavelet transforms if  $\tau$  and  $a$  are discrete. The

drawback of the CWT is that the representation of the signal is often redundant.

Since  $a$  and  $\tau$  are continuous over  $\mathbb{R}$  (all real number). The original signal can be reconstructed completely by a sample version of  $W_f(a, \tau)$ . Sample  $W_f(a, \tau)$  is in a dyadic grid, i.e.,

$$a = 2^{-m} \quad \text{and} \quad \tau = n2^{-m} \quad m, n \in \mathbb{Z} \quad \text{and} \quad m, n \in (-\infty, \infty)$$

And Eq. (2) can be rewritten as

$$W_f(m, n) = 2^{m/2} \int_{-\infty}^{\infty} x(t) \psi^*(2^m t - n) dt = \int_{-\infty}^{\infty} x(t) \psi_{m,n}^*(t) dt \quad (3)$$

Where  $\psi_{m,n}(t)$  is the dilated and translated version of the mother wavelet  $\psi(t)$ .

Two orthogonal functions (scaling and wavelet functions) are used to decompose the frequency information into low and high-frequency components in the wavelet transform. With the choice of  $a$  and  $\tau$ , there exists the multiresolution analysis (MRA) algorithm, which decompose a signal into scales with different time and frequency resolution. The MRA is designed to provide good time resolution and poor frequency resolution at high frequencies (through the wavelet function), and good frequency resolution and poor time resolution at low frequencies (through the scaling function). Therefore, the original signal can be separated systematically into different frequency bands.

A wave of any shape can be used as a mother wavelet if it is localized at a particular time. Several families such as Harr, Daubechies, Biorthogonal, Morlet and Mexican hat have been proven and widely used (Mallat 1999). However, a universal criterion does not exist for selecting an optimal wavelet function for a given application. In the following discussion, the Daubechies wavelet family (dbN) is chosen to complete the analyses, where N is the order of the wavelet. These wavelets have no explicit expression except for db1, which is the Haar wavelet, and are compactly supported wavelets with extreme phase and the highest number of vanishing moments for a given support width (Misiti *et al.* 2007).

A vanishing moment limits the wavelet's ability to represent polynomial behavior or information in a signal. For example, db1, with one moment, can easily encode polynomials of one coefficient, or constant signal components. db2 encode polynomials with two coefficients, i.e. constant and linear signal components; and db3 encodes 3-polynomials: i.e. constant, linear and quadratic signal components. So, one can improve the multiple resolution of the signal by increasing the N value. db1 to db10 are the most commonly used. For the Daubechies orthogonal wavelets, the higher the level it is, the narrower the frequency bandwidth can be decomposed to. Therefore, db10 is used in this study, and it is able to decompose the raw signal into 8 different frequency levels.

### 3. Pile integrity test procedure

The evaluation of pile integrity includes two major parts: the evaluation of pile length and the evaluation of defect location. The wavelet analysis for the impulse response of pile will be introduced to apply to the following two parts.

#### 3.1 Evaluation of pile length

When determining the pile length using the impulse response method, the reflected signal from the pile tip usually suffers interference from high-frequency noise. With the MRA characteristics of DWT, it is able to decompose the signal into multiple orders (layers), which in this case is 8 layers, as shown in Fig. 3 where (a) is the approximation signal and (b) is the detail signal. As can be seen in Fig. 3, the d1 and d2 layers are considered as noise. Fig. 4(a) is the original signal in the frequency domain. The noise can be determined by transforming the layers of signals into frequency domain and then finding out the range of frequencies that are considered as noise, and in this case, this range is above 20 kHz, as shown in Fig. 4(c). Moreover, the mechanical admittance curve is obtained by dividing the velocity spectrum (Fig. 4(c)) by the force spectrum (Fig. 4(d)), so their range has to be the same. Fig. 4(c) shows that the frequency range of d1 and d2 (noise) falls between 20 kHz and 50 kHz, while Fig. 4(d) shows that the frequency range falls between 0 kHz to 20 kHz. Therefore, this paper considers the signal to be noise if they are greater than 20 kHz. Layers d1 and d2 were then filtered out from the eight layers, and the remaining six layers were then stack back together to finish the filtering, and the results are shown in Fig. 4(b). Then, the impulse response method can be applied to the de-noised layer signal to determine pile length by finding periodically repeated peaks and finding frequency difference  $\Delta f$ . Finally, Eq. (3) is used to determine the estimated pile length.

The conventional impulse response method is already able to estimate pile length up to 95% accuracy, which already satisfies engineering requirements. The filtering does not affect the results too significantly, therefore, the accuracy of estimating pile length will not be further discussed in this paper.

#### 3.2 Evaluation of pile flaws

Compared with using filtered signals to estimate pile length, finding defects on the pile is much more difficult. The wavelength of the impulse stress wave is usually too long meaning that it will skip the defect because most defects are small. Previous studies state that the defects with an area ratio under 10% are very difficult to detect because their reflected signals are too weak compared to the reflected signals from a pile tip (Lin *et al.* (1991), Baker *et al.* (1991) and Kim *et al.* (2002)). This paper uses the MRA characteristic of DWT to decompose the signal into different layers using different scales, then, in each detail layer, the IR method is used to analyze the reflected signal.

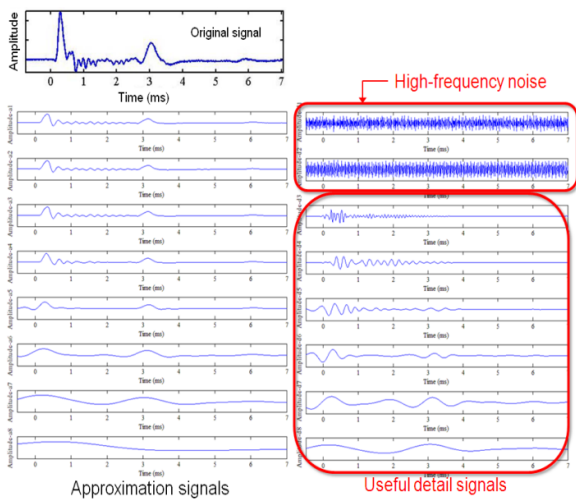


Fig. 3 Approximation signal and detail signal with db10

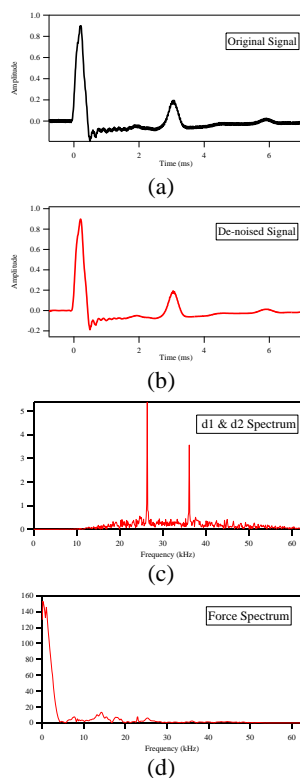


Fig. 4 (a) Original signal (S), (b) De-noised signal (Ds), (c) Noise spectrum and (d) Force spectrum

The defect signals are unidentifiable in raw time domain data. Through DWT decomposition, the decomposed signal can be divided into detail signal (dN) and approximating signal (aN), through wavelet function and scaling function, respectively. The letter N represents the level of decomposition. Signals in higher levels have a lower frequency. The approximation signal is the low-frequency portion that looks similar to the original signal. Some of the lower level approximation signals (layers) are also eliminated because they are too similar to the original signal and are not likely to contain defect signals. As from the

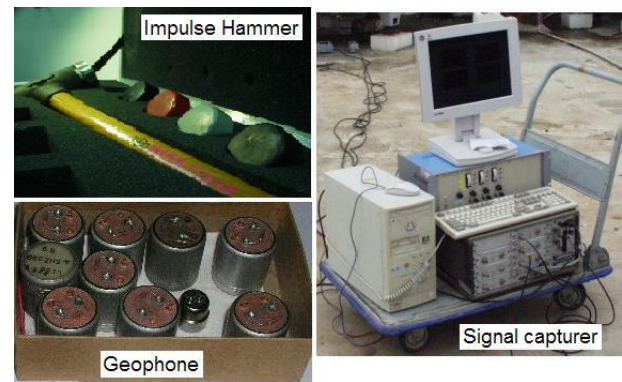


Fig. 5 Test equipment

previous section, layers d1 and d2 are eliminated because they are considered as noise. Therefore, only layers d3 through d8 are considered as defect signals containing layers. The IR method is more easily used to analyze these layers to estimate the location of defects.

The IR method analyzes the raw signal using DWT method, which is summarized as follow:

Step 1: Choosing the mother wavelet and numbers of decomposed levels. In this study, db10 mother wavelet and 8 decomposed levels are used.

Step 2: With the MRA characteristics of DWT, the raw signal of time domain, which is analyzed by the chosen mother wavelet and levels in step 1, is decomposed to approximation signals and detail signals.

Step 3: The noises can be determined and filtered out from detail signals. Using the residual signals to reconstruct the new signal can be easier applied in IR method to estimate the pile length. (The residual signals are reconstructed into new signals, which are easier to apply in IR methods to estimate pile length.)

Step 4: As from the previous point, other detail signals are considered as defect signals containing layers. The IR method is used to analyze these layers and the defect can easily be found.

#### 4. Testing equipment

To obtain a high-quality signal from the in-situ sonic echo test, an optimal configuration of a hammer force source, a sensor, and a signal capture facility are needed. A typical set of equipment is shown in Fig. 5. The equipment consists of a calibrated impulse hammer, geophone sensors, and a computer-controlled signal capturer (signal analyzer). The details of the equipment are listed below.

- (1) Sensor: The model-L28B Geophone (works as signal receiver), with natural frequency of 4.5 Hz, is produced by Mark Product, U.S.A. To ensure the geophone is in good coupled with the top of the pile, gypsum is used as the bonding agent so that the stress waves can completely transmit to the geophone.
- (2) Signal analyzer: The model HP35650A analyzer is a multi-tasking computer. The measurement hardware is combined with the application software. The hardware capture signals both in time and frequency domains and

the measurement data for a large number can be easily configured. The sampling rate of the system is set to 102.4 kHz to make sure that the high-frequency data will not be cut off.

Impulse hammer: The model-086D20 short-sledge impulse hammer made by PCB Piezotronics, Inc., USA, is used to create the pulse source. The hammer’s resonant frequency is approximately 12 kHz, and the sensitivity is 0.23 mV/N.

### 5. Case study

Three precast hollow piles were placed in a field adjacent to the Department of Civil Engineering building at the National Cheng Kung University. All three hollow piles are 6 m long and have an outer-diameter of 30 cm and an inner-diameter of 17 cm. Defects of different types and shapes were added during their construction for the purpose of this study. Pile 1 has a 10 cm long circular necking at a depth of 5.1 m, and the area ratio of the necking is 30%. Pile 2 has two necks at a depth of 3.3 m and 5.1 m, with area ratios of 5% and 10%, respectively. Finally, Pile 3 has two rectangular openings opposite to each other; the higher opening measuring 7.4 cm by 15 cm is 3.3 m deep, and the lower opening is 22 cm by 15 cm at a depth of 5.1 m. Detailed dimensions of the piles and their defects are shown in Fig. 6 and Table 3.

The profile of the soil surrounding the piles is as follows: The depth from 0 m to 0.9 m is fills, depth from 0.9 m to 3.8 m is classified as SM, depth from 3.8 m to 6.3 m is classified as ML, and depth from 6.3 m to 13.6 m is classified as SM. It is clear that there are three layers of soil surrounding the testing pile. The interfaces between each soil layer are located at depth of 0.9 m and 3.8 m, respectively.

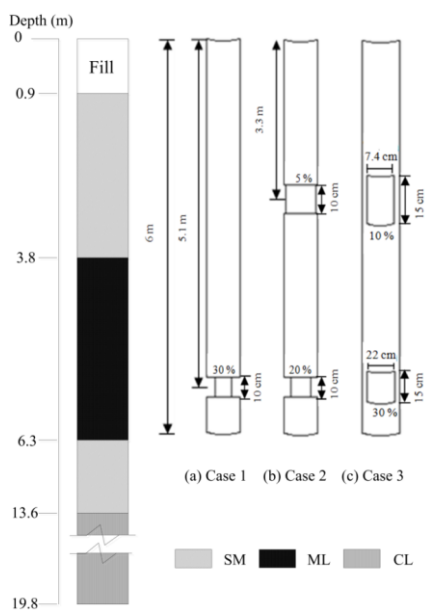


Fig. 6 Soil profiles of the test site and the profiles of testing piles

Table 3 Profiles of pile designed for the case study

Pile no.	Pile length (m)	Pile diameter (cm)	Flaw depth (m)	Flaw size (%)	Flaw type
1	6	Outer 30	5.1	30	Annular necking
		Inner 17			
2	6	Outer 30	3.3	5	Annular necking
		Inner 17	5.1	20	Annular necking
3	6	Outer 30	3.3	10	Rectangular void
		Inner 17	5.1	30	Rectangular void

#### 5.1 Pile no. 1

The test results for Pile no. 1 are shown in Fig. 7. When comparing the soil profiles of the location, it is evident that layers d3, d7 and d8 are of different confined conditions, which means different soil layers, but the depth of the soil interfaces did not coincide exactly with the boring log.

There are two possible causes of this error: the signal itself or the slide inclination of the soil layers. Furthermore, the results show that the interface estimation of the shallow soil layer is more accurate than that of deep soil layer, which is because the energy produced by the impulse hammer dissipates as it travels down the length of the pile. However, the pile tested is only 6 m long, so only the top two soil layers have been considered in this study.

Layers d4, d5, and d6 were chosen to find the defect and its location. Because the results are very similar, the average value of the three layers was taken to perform the analysis. The estimated depth of the defects from layers d4, d5, and d6 was found to be 5.22 m, which has an error rate of 2.4% compared to the actual depth. This proves that DWT-based IR method is good for detecting defects that are larger than 30%.

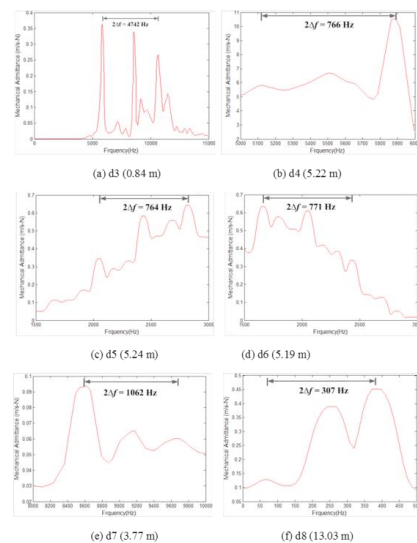


Fig. 7 Frequency responses of different detail levels of the db10 in pile no. 1

It is interesting to note that, in layers d3, d5, and d6, there are some peaks appearing beside the dominant frequency. They are probably caused by the flexural vibration that is produced by the eccentric loading when force is applied to the side of the pile (Fei *et al.* 2007). According to the study, this so-called “bending vibration effect” can be minimized when the sensor and impulse source (where the hammer strikes the pile) form a 90-degree angle. Although the bending vibration effect can be minimized, it cannot be completely eliminated.

When finding the periodically repeated peaks in the mobility curves, this study required three peaks to be chosen to ensure that they were actually periodically repeated, and the error rate of  $\Delta f$  of these three peaks was required to be within 5% to minimize the chance of people misinterpreting the data.

Compared to the traditional IR method, the DWT-based IR method can provide an easier means of analyzing the data by decomposing the signal into many layers.

5.2 Pile no. 2

In contrast to Pile no. 1, which had only one large defect, Pile no. 2 had two smaller defects (5 % and 20 %) at different depths. There are two reasons why Pile no. 2 was designed this way: 1. to see if the DWT-based IR method is able to detect very small defects (5%), and, 2. to test this method’s ability to find multiple defects in one pile.

The test results for Pile no. 2 are shown in Fig. 8. Layer d3 indicates an impedance change at a depth of 3.12 m, which has an error rate of 5.5% compared to the actual defect depth of 3.3 m.

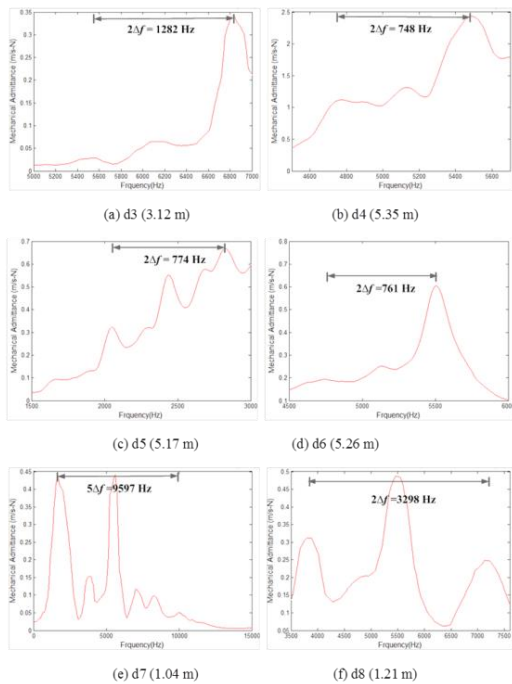


Fig. 8 Frequency responses of different detail levels of the db10 in pile no. 2

The results for layers d4, d5, and d6 are very similar, so an average value was calculated. The averaged result shows a defect at a depth of 5.26 m, with an error rate of 3.1% compared to the actual defect depth of 5.1 m. Finally, layers d7 and d8 show the interface of the two soil layers on the top, and the average depth is 1.13 m.

The results for Pile no. 2 are not as good when compared to the results in Pile no. 1, and the soil layer interface at a depth of 3.8 m could not be found. The dissipation rate of the stress wave increased as the number of defects increased, so the reflected signal was not as strong and clear as in Pile 1.

The reflected signal from the small defect at a depth of 3.3 m is weaker than the large defect at a depth 5.1 m, so most of the MRA analysis methods can only pick up the reflected signal from large defects. However, the DWT-based IR method is able to extract the reflected signal from the small defect. This proves that this method can successfully reduce the influence of defect size on the estimation of defect location.

5.3 Pile no. 3

The defects of Pile no. 3 are two square openings. They have the same depth as the circular necking in Pile 2, but the defect area ratios are increased to 10% and 30%. This case was designed to test the applicability of the DWT-based IR method in detecting different defect forms. The Pile no. 3 results are shown in Figure 9. As in the other examples, the results from layers d3, d5, and d8 are similar, so the average value of the three was used. The defect depth was estimated to be 5.20 m from the average of d3, d5, and d8, which was a 2% error from the actual defect location. Layer d6 detected an impedance change at a depth of 3.39 m and had a 2.7% error from the actual 3.3 m deep defect. Finally, layers d4 and d7 averaged to a depth of 1.02 m and had a 13% error rate from the depth of the interface of the soil layers.

The form and shapes of the defects does not affect the results significantly, as can be seen in this case. This means that the DWT-based IR method is appropriate for detecting these kinds of defects.

The summary of pile length and flaw location evaluated is listed in Table 4. As shown in the Table 4, the test results show that the satisfactory results can be obtained for both pile length and defect location using the suggested analysis method.

Table 4 Pile length and flaw evaluated and its error comparing with designed value

Mother Wavelet	Levels	Case	Pile length (m)	Error (%)	Flaw location (m)	Error (%)
db10	8	1	6.04	0.63	5.22	2.4
		2	5.77	3.82	3.12	5.5
		3	5.97	0.53	5.26	3.1
						3.39
					5.2	2

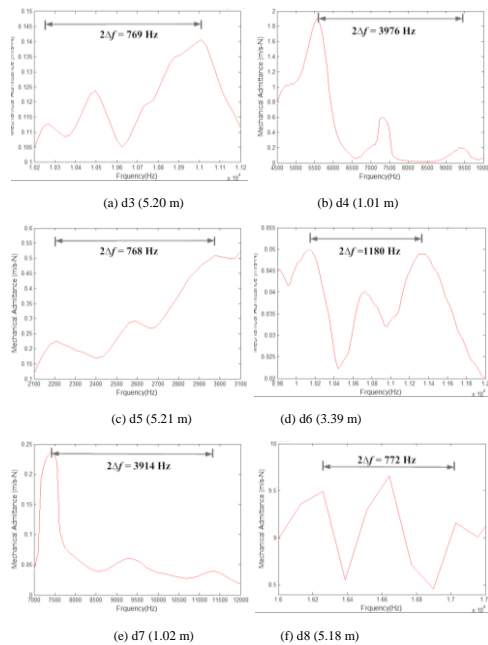


Fig. 9 Frequency response of different detail levels of the db10 in pile no. 3

## 6. Conclusions

The sonic echo and impulse response methods can successfully determine the length of the isolated piles. Testing results show that the sonic echo test is good to define the length of the pile, but it is not exact to define the defect location. The reason could be due to that the defect location is placed too close to the bottom of the pile or the reflected signal is too small compared to the signal reflected back from pile tip. Application of wavelet analysis with the impulse response signals can effectively separate noise, defect signal, and the signal reflected from the bottom of the testing pile. It is much easier to infer the defect location using the individual frequency plot from the decomposed signals. Wavelet transform-based impulse response method presented in this paper is able to estimate the pile length with percentage error less than 5%. This proves that the suggested method is an effective tool to determine pile length even if the piles are with small defects or existing significant soil interface. Otherwise, DWT-based IR method can also detect the location of defects with area ratio under 10%. Furthermore, the interface of soil layers can also be determined. With the aid of boring log., the impedance change due to different soils can be eliminated, and thus makes it easier to determine which layer contains pile defect signals.

## Acknowledgments

The research described in this paper was financially supported by the Natural Science Council of Republic of China under grant number NSC 102-2221-E-006-206. Grateful appreciation is expressed for this support.

## References

- Addison, P.S. (2002), *The Illustrated Wavelet Transform Handbook*, Institute of Physics.
- Baker Jr., C.N., Drumright, E.E., Mensah, F., Parikh, G. and Ealy, C. (1991), "Use of nondestructive testing to evaluate defects in drilled shafts", *Transportation Research Record*, **1331**, 28-35.
- Beheshti-Aval, S.B., Taherinasab, M. and M. Noori, M. (2011), "Using harmonic class loading for damage identification of plates by wavelet transformation approach", *Smart Struct. Syst.*, **8**(3), 253-274.
- Berger, J.A. and Cotton, D.M. (1990), "Low strain integrity testing of deep foundations", *Proceedings of the 5th Annual Members' Conference*, Seattle.
- Briaud, J.L., Ballouz, M. and Nasr, G. (2002), "Defect and length predictions by NDT methods for nine bored piles", *International Perspective on Theory, Design, Construction, and Performance*, Orlando, Florida, USA.
- Fei, K., Liu, H.L. and Zhang, T. (2007), "Three-dimensional effects in low strain integrity test of PCC pile", *Rock Soil Mech.*, **28**, 1095-1102.
- Finno, R.J. and Gassman, S.L. (1998a), "Evaluation of bridge foundations by impulse response methods", *Structural Materials Technology III*, San Antonio, Texas, USA.
- Finno, R.J. and Gassman, S.L. (1998b), "Impulse response evaluation of drilled shafts", *Journal of Geotechnical and Geoenvironmental Engineering*, **124** (10), 965-975.
- Harrell, A.S. and Stokoe, K.H., II, (1984), *Integrity Evaluation of Drilled Piers by Stress Waves*, Transportation Research Center, The University of Texas at Austin.
- Hartung, M., Meier, K. and Rodatz, W. (1992), "Integrity testing on model pile", *Proceedings of the 4th International Conference on the Application of Stress-Wave Theory to Piles*, Netherlands.
- Huang, Y.H., Ni, S.H., Lo, K.F. and Charn, J.Y. (2010), "Assessment of identifiable defect size in a drilled shaft using sonic echo method: Numerical simulation", *Comput. Geotech.*, **37**(6), 757-765.
- Huang, Y.H. (2011), "Evaluation of the stress wave techniques for the integrity test of pile foundations", *Ph. D. Dissertation*, Natl. Cheng Kung Univ., Tainan, Taiwan.
- Iskander, M., Roy, D., Kelley, S. and Ealy, C. (2003), "Drilled shaft defects: detection, and effects on capacity in varved clay", *J. Geotech. Geoenviron. Eng. - ASCE*, **129**(12), 1128-1137.
- Kim, D.S., Kim, H.W. and Kim, W.C. (2002), "Parametric study on the impact-echo method using mock-up shafts", *NDT&E Int.*, **35**(8), 595-608.
- Kim, D.S. and Kim, H.W. (2004), "Evaluation of the base condition of drilled shafts by the impact-echo method", *Geotech. Test. J.*, **27**(5), 496-503.
- Lin, Y., Sansalone, M. and Carino, N.J. (1991), "Impact-echo response of concrete shafts", *Geotech. Test. J.*, **14** (2), 121-137.
- Malhotra, V.M. (1976), *Testing Hardened Concrete: Nondestructive Methods*, Iowa State University Press.
- Mallat, S. (1999), *A wavelet tour of Signal Processing*. Academic, San Diego, 2nd edition.
- Misiti, M., Misiti, Y., Oppenheim, G. and Poggi, J.M., (Eds.) (2007), *Wavelets and Their Applications*, ISTE Ltd., DSP series.
- Newland, D.E. (1999), "Ridge and phase identification in the frequency analysis of transient signals by harmonic wavelets", *J. Vib. Acoust.*, **121**(2), 149-155.
- Ni, S.H., Huang, Y.H. and Lo, K.F. (2011), "Estimating the flaw size in drilled shafts using an impulse response method", *J. Civil Eng. - KSCE*, **38**(1), 127-132.
- Ni, S.H., Isenhowe, W.M. and Huang, Y.H. (2012), "CWT technique for low-strain integrity testing of deep drilled shafts", *J. Geoen.*, **7**(3), 97-105.

- Park, H.C. and Kim, D.S. (2001), "Evaluation of the dispersive phase and group velocities using harmonic wavelet transform", *NDT & E Int.*, **34**(7), 457-467.
- Sarhan, H.A., O'Neill, M.W. and Hassan, K.M. (2002), "Flexural performance of drilled shafts with minor flaws in stiff clay", *J. Geotech. Geoenviron. Eng.*, **128**(12), 974-985.
- Stain, R.T. (1982), "Integrity testing", *Civil Engineering*, April, 53-59.

CC